Electronic Supplementary Material (ESI) for Energy & Environmental Science

Supplementary Information

Layered corrugated electrode macrostructures boost microbial bioelectrocatalysis

Shuiliang Chen [1], Guanghua He [1], Qin Liu [1], Falk Harnisch [2], Yan Zhou [1], Yu Chen [1], Muddasir Hanif [1], Suqin Wang [1], Xinwen Peng [1], Haoqing Hou[1]*, Uwe Schröder [2]*

[1] *Dept of Chemistry and Chemical Engineering, Jiangxi Normal University, Nanchang, 330022, China;*
[2] *Institute of Environmental and Sustainable Chemistry, Technische Universität Braunschweig, Hagenring 30, 38106 Braunschweig, Germany;*

corresponding authors: uwe.schroeder@tu-bs.de; hqhou01@yahoo.com;

Material composition and material properties

The morphology of LCC as observed under scanning electron microscope (SEM) is shown in Fig.S1. It shows that the LCC is composed of a fiber network.

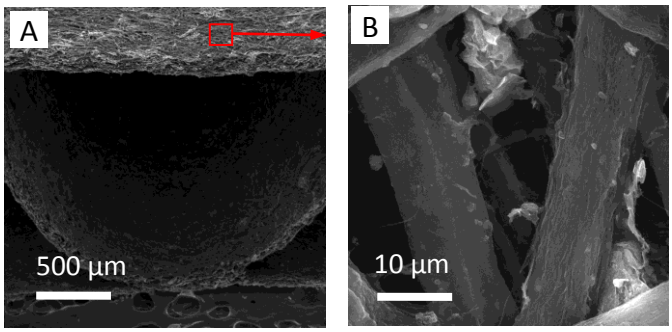

Figure S1 A) and **B)** Scanning electron microscopy images of layered corrugated carbon at different magnifications, (single-LCC, H_f = 2.9 mm)

In order to assure that no unwanted chemical impurities influence the carbonized LCC, a chemical analysis based on energy dispersive x-ray (EDX) was performed. The spectra and the resulting analysis (Fig. S2) reveal that the samples do not contain remarkable transition metal impurities that may affect the bio-anode performance. The major constituents of LCC beside carbon is oxygen, which illustrates a not entirely complete carbonization of the precursor material. The further impurities, i.e., Na, Mg, Al, Si, S and Ca have their basis in the composition of plant biomass, the original precursor of paper. These elements are naturally not removed upon the pyrolysis procedure.

A

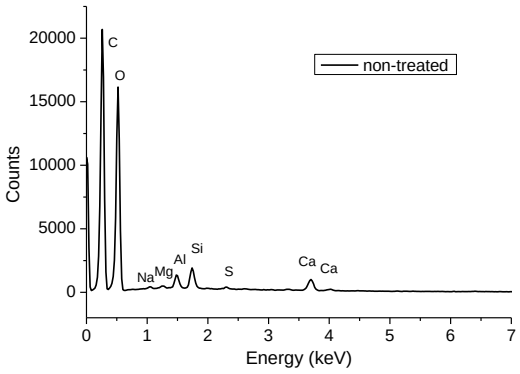

B

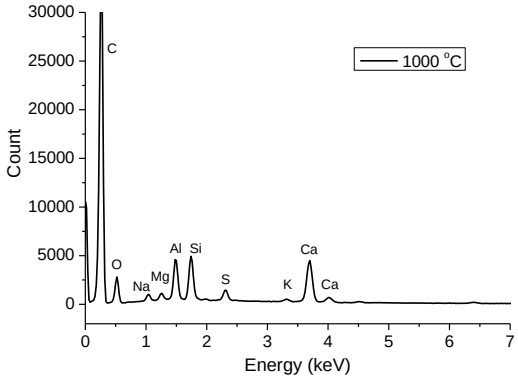

C

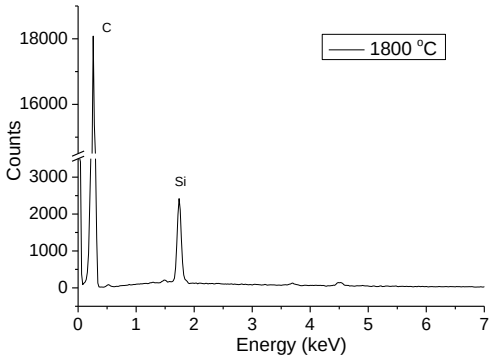

	Cardboard Atom %	**LCC-1000°C** Atom %	**LCC-1800°C** Atom %
C	51.49	81.36	97.2
O	46.99	13.50	0.91
Na	0.11	0.33	-
Mg	0.08	0.24	-
Al	0.36	1.16	0.05
Si	0.54	1.28	1.66
S	0.05	0.34	-
Ca	0.36	1.56	0.05

Figure S2. Energy dispersive X-ray (EDX) spectrum and element content of the non-carbonized cardboard (A) LCC carbonized at 1000 °C (B) and LCC carbonized at 1800 °C (C), and tabular summary of the elemental composition.

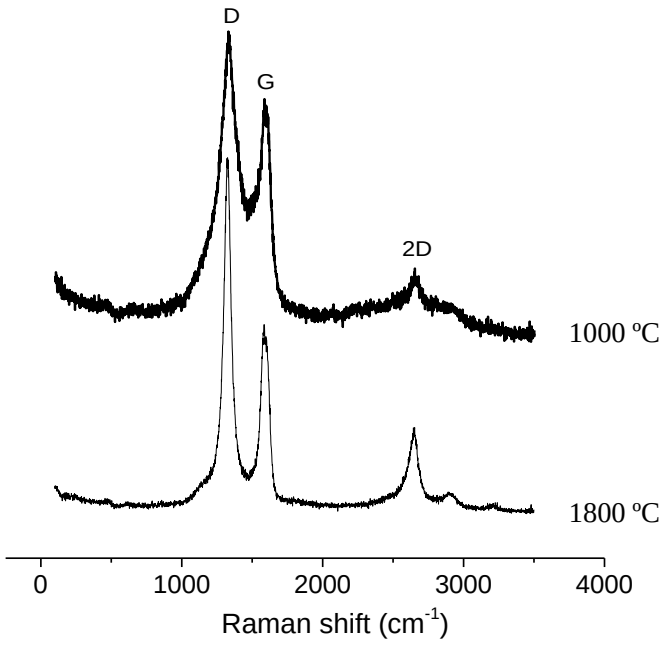

Figure S3. Raman spectra of LCC samples carbonized at 1000 °C and 1800 °C

Raman and wide angle x-ray diffraction (WXRD) analyses were conducted to investigate the characteristics of the electrode material. The Raman spectra of LCC, carbonized at 1000 °C (Fig. S3) show that LCC is composed of disordered turbostratic (1327 cm^{-1}) and ordered graphitic structures (1580 cm^{-1}).

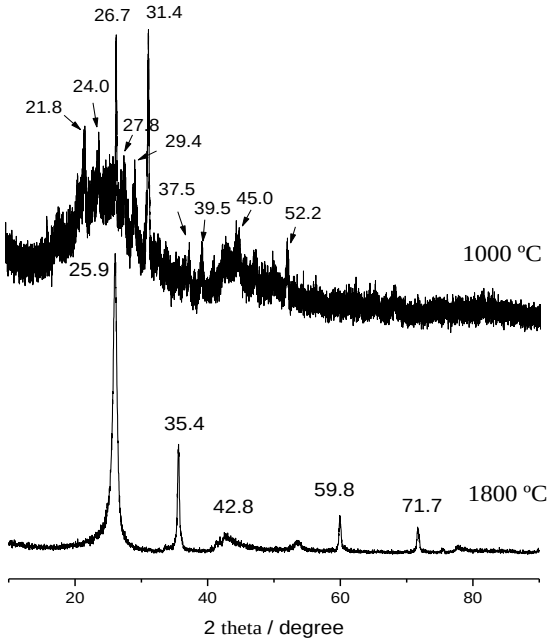

Figure S4. XRD curves of LCC samples carbonized at 1000 °C and 1800 °C

As displayed in WXRD curves in Fig. S4 for LCC carbonized at 1000°C, except for the wide peak of carbon range from 15° to 35° which have to be assigned to graphite, plenty of sharp peaks are shown. According to the EDX element analysis and the XRD spectra database, these peaks belong to silicates and aluminates, mainly Al_2O_3 (21.8, 27.8, 31.4 and 45.0), $NaAlSi_3O_8$ (24.0, 26.7 and 27.8), $Mg_2Al_4Si_5O_{18}$. (20.9, 27.8, 29.4 and 31.4). For the LCC sample carbonized at 1800 °C, the peaks are attributed to ordered graphite (25.9, 42.8 and 71.7) and to SiC (35.4 and 59.8)

As Fig. S2C shows a higher carbonization temperature (1800°C) significantly reduces the content of oxygen and other elements such as sulfur and sodium down to few percent. As Table S1 illustrates, however, this does not improve the bioelectrochemical performance of the resulting electrode material. Single layer LCC-2.9 electrodes carbonized at 800, 900, 1000 and 1800 °C delivered similar current densities of around 7.0 mA cm^{-2}. For this study, a carbonization temperature of 1000 °C was chosen. Yet, from the energy investment point of view, the carbonization temperature can certainly be further reduced.

Table S1: Bioelectrocatalytic current density of LCC-2.9 electrodes carbonized at different temperature

Carbonization temperature (°C)	**H_e (mm)**	**W (mm)**	**L (mm)**	**$j_{projected}$ (mA cm^{-2})**
°C	mm	mm	mm	mA cm^{-2}
800	2.9	10	10	6.89
900	2.9	10	10	7.34
1000	2.9	10	10	7.28
1800	2.9	10	10	7.03

To remove the further inorganic constituents the resulting electrode materials were treated with sulfuric acid. This removed most elements, except for silica and oxygen. Since this treatment did not have an effect on the electrochemical performance, all electrodes in this study were used without purification.

Further bioelectrochemical electrode characterization

A complete summary of the experimental bioelectrochemical data is presented in Table S2. It provides an overview on the absolute currents, the projected, geometric and volumetric current density data.

Table S2: Summary of the geometric and performance data of the electrode materials used in this study

	n	H_e	*W*	*L*	$A_{geom.}$	$i_{absolute}$	$j_{projected}$		$j_{geometric}$		$j_{volumetric}$
		mm	mm	mm	cm^2	*mA*	mA cm^{-2}	*(A m^{-2})*	mA cm^{-2}	*(A m^{-2})*	mA cm^{-3}*
Graphite rod	-	-	10	10	1	1.10 ± 0.08	1.10 ± 0.08	(11)	1.10 ± 0.08	(11)	-
Carbon felt	-	2	10	10	*n.a.**	1.60 ± 0.06	1.60 ± 0.06	(16)	*n.a.*	*n.a.*	8.0 ± 0.3
LCC, Liner only	0	0.15	10	10	1	1.38 ± 0.11	1.38 ± 0.11	(13.8)	1.38 ± 0.11	(13.8)	-
LCC-1.4	1	1.4	10	10	5.83	4.68 ± 0.35	4.68 ± 0.35	(46.8)	0.80 ± 0.06	(8.0)	33.4 ± 2.5
	1	1.4	10	8.1	4.72	4.33 ± 0.26	5.35 ± 0.32	(53.5)	0.92 ± 0.05	(9.2)	38.2 ± 2.3
	1	1.4	10	5.2	3.03	2.9 ± 0.20	5.58 ± 0.39	(55.8)	0.96 ± 0.06	(9.6)	39.9 ± 2.8
	1	1.4	10	3.1	1.81	2.1 ± 0.14	6.77 ± 0.46	(67.7)	1.16 ± 0.08	(11.6)	48.4 ± 3.3
LCC-2.2	1	2.2	10	10	5.83	7.02 ± 0.52	7.02 ± 0.52	(70.2)	1.20 ± 0.09	(12.0)	31.9 ± 2.4
	1	2.2	10	8.2	4.78	6.37 ± 0.30	7.77 ± 0.37	(77.7)	1.33 ± 0.06	(13.3)	35.3 ± 1.7
	1	2.2	10	5.3	3.09	4.19 ± 0.27	7.91 ± 0.51	(79.1)	1.38 ± 0.08	(13.8)	36.0 ± 2.3
LCC-2.9	1	2.9	10	10	5.83	7.28 ± 0.52	7.28 ± 0.52	(72.8)	1.25 ± 0.09	(12.5)	25.1 ± 1.8
	1	2.9	10	8.5	4.95	6.69 ± 0.30	7.87 ± 0.35	(78.7)	1.35 ± 0.05	(13.5)	27.1 ± 1.2
	1	2.9	10	5	2.91	4.12 ± 0.26	8.24 ± 0.51	(82.4)	1.41 ± 0.08	(14.1)	28.4 ± 1.8
Double-LCC-2.9	2	5.4	10	10	10.66	15.7 ± 0.61	15.71 ± 0.61	(157.1)	1.44 ± 0.10	(14.4)	29.1 ± 1.1
Triple-LCC-2.9	3	8.2	10	10	15.49	19.8 ± 1.05	19.75 ± 1.05	(197.5)	1.28 ± 0.14	(12.8)	24.1 ± 1.3
Hexa-LCC-2.9	6	18	42	9.2	115.81	151.1 ± 6.0	39.1 ± 1.55	(391.3)	1.31 ± 0.08	(13.1)	21.7 ± 0.9

n denotes the number of flute layers; H_e denotes the electrode height with $H_e = H_f * n$; *W* and *L* denote the width and length of the electrode, respectively.

The experimental setup used in this study is based on an immersion of the respective electrodes into a slightly stirred electrolyte/substrate solution with subsequent biofilm growth and performance testing. Thus, the LCC channels were not subject of direct flow-through but rather passive mass transfer. The actual potential of the LCC structure becomes visible when the electrode length, i.e., the flute channels' length and thus the mass-transfer pathway within the electrode channels, is reduced from 10 mm to around 5 or 3 mm (see Table S2). Here, the maximum projected current density increases for all channel widths to $j_{projected}$ = 6.8 mA cm^{-2} (LCC-1.4), $j_{projected}$ = 7.91 mA cm^{-2} (LCC-2.2) and 8.2 mA cm^{-2} (LCC-2.9). At the same time, the geometric current density of these electrodes increases to reach the value of the pure LCC liner, about $j_{geometric}$ = 1.38 mA cm^{-2}. This leads to the expectation that in a flow-through fuel cell setup that can more efficiently utilize the channel structure of the LCC a further increase of the electrode performance can be achieved.

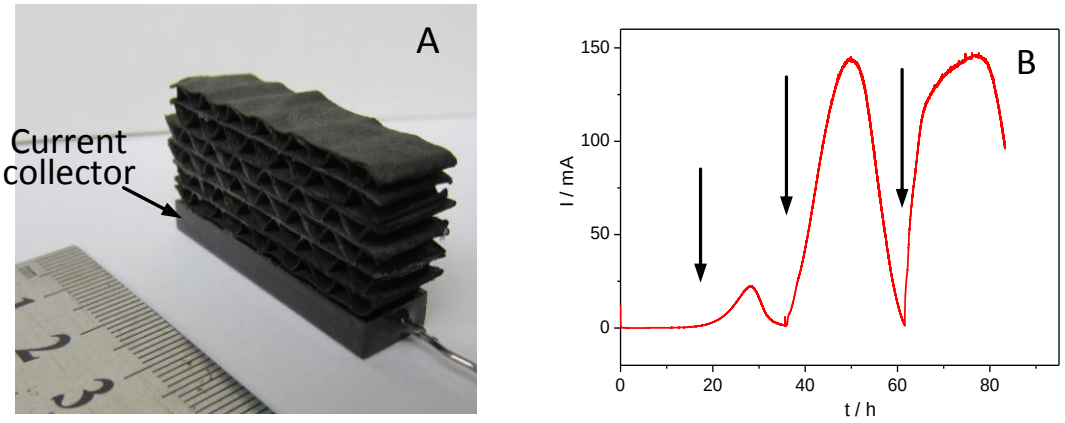

Figure S5 (A) Digital photograph of a six-layer LCC electrode (*hexa*-LCC-2.9) and (B) semi batch current generation curve. The arrows represent replenishment of substrate with 20mM sodium acetate